Microtubule polymerase and processive plus-end tracking functions originate from distinct features within TOG domain arrays

Brian D. Cook[a], Fred Chang[b], Ignacio Flor-Parra[c,*], and Jawdat Al-Bassam[a,*]
[a]Department of Molecular Cellular Biology, University of California, Davis, Davis, CA 95616; [b]Department of Cell and Tissue Biology, University of California, San Francisco, San Francisco, CA 94143; [c]Centro Andaluz de Biología del Desarrollo, Universidad Pablo de Olavide/CSIC/Junta de Andalucía, 41013 Seville, Spain

ABSTRACT XMAP215/Stu2/Alp14 accelerates tubulin polymerization while processively tracking microtubule (MT) plus ends via tumor overexpressed gene (TOG) domain arrays. It remains poorly understood how these functions arise from tubulin recruitment, mediated by the distinct TOG1 and TOG2 domains, or the assembly of these arrays into large square complexes. Here, we describe a relationship between MT plus-end tracking and polymerase functions revealing their distinct origin within TOG arrays. We study Alp14 mutants designed based on structural models, with defects in either tubulin recruitment or self-organization. Using in vivo live imaging in fission yeast and in vitro MT dynamics assays, we show that tubulins recruited by TOG1 and TOG2 serve concerted, yet distinct, roles in MT plus-end tracking and polymerase functions. TOG1 is critical for processive plus-end tracking, whereas TOG2 is critical for accelerating tubulin polymerization. Inactivating interfaces that stabilize square complexes lead to defects in both processive MT plus-end tracking and polymerase. Our studies suggest that a dynamic cycle between square and unfurled TOG array states gives rise to processive polymerase activity at MT plus ends.

Monitoring Editor
Thomas Surrey
The Francis Crick Institute

Received: Feb 8, 2019
Revised: Apr 2, 2019
Accepted: Apr 5, 2019

INTRODUCTION

Microtubules (MTs) are dynamic polymers that drive diverse cellular functions such as mitosis, cell motility, and organelle transport. MTs polymerize from soluble αβ-tubulin dimers (herein termed αβ-tubulins) via assembly into protofilaments at MT ends (Akhmanova and Steinmetz, 2015). Guanosine-5′-triphosphate (GTP) hydrolysis is activated by head-to-tail αβ-tubulin polymerization, leading to stochastic transitions from polymerization to depolymerization at MT plus ends, termed dynamic instability (Akhmanova and Steinmetz, 2011, 2015). The XMAP215/Stu2/Alp14 proteins constitute a core and conserved class of regulators that accelerate MT polymerization and as such are termed MT polymerases. MT polymerases are universally essential for MT dynamics across eukaryotes. If inactivated or depleted, cells exhibit slow MT polymerization and fewer MTs, resulting in the formation of abnormally small mitotic spindles leading to defects in chromosome segregation (Al-Bassam and Chang, 2011; Akhmanova and Steinmetz, 2015).

XMAP215/Stu2/Alp14 proteins function by recruiting and releasing soluble αβ-tubulins via highly conserved arrays of tumor overexpressed gene (TOG) domains (Al-Bassam and Chang, 2011; Brouhard and Rice, 2014). Each of these array consists of tandem sets of TOG domains numbered with respect to their positions from each protein's N-terminus. Each TOG domain represents a unique class that is conserved with respect to their position in the sequence across multiple species (Al-Bassam and Chang, 2011). Yeast MT polymerases, such as Alp14 and Stu2, contain an array consisting of TOG1 and TOG2 domains, followed by a positively charged Ser-Lys-rich (SK-rich) region and a C-terminal coiled-coil domain, leading to homodimers with four TOG domains (Al-Bassam *et al.*, 2006; Haase *et al.*, 2018). *Xenopus* XMAP215 and human ch-TOG consist of an array of five TOG domains and

This article was published online ahead of print in MBoC in Press (http://www.molbiolcell.org/cgi/doi/10.1091/mbc.E19-02-0093) on April 10, 2019.

*Address correspondence to: Jawdat Al-Bassam (jawdat@ucdavis.edu) and Ignacio Flor-Parra (iflopar@upo.es).

Abbreviations used: GFP, green fluorescent protein; GTP, guanosine-5′-triphosphate; MBC, MT inhibitor methyl 2-benzimidazolecarbamate; mNG, mNeonGreen; MT, microtubule; SK-rich, Ser-Lys-rich; TIRF, total internal reflection; TOG, tumor overexpressed gene.

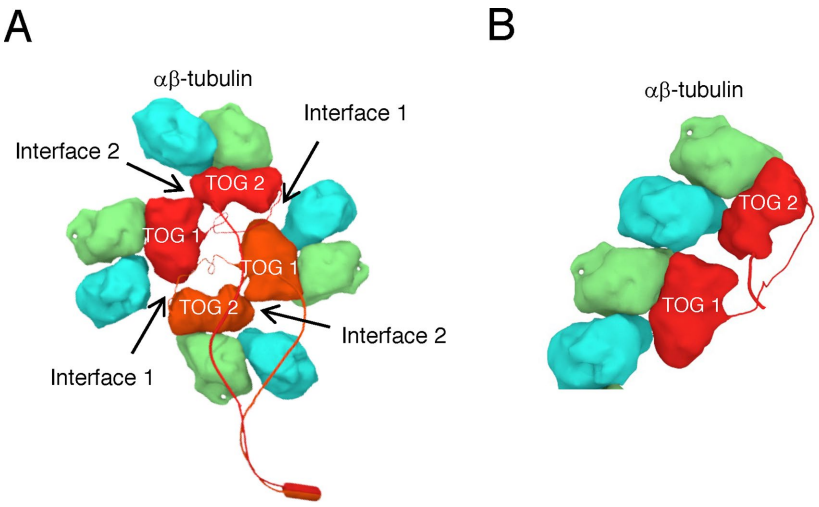

FIGURE 1: Structures of the αβ-tubulin structures of TOG1-TOG2 arrays. (A) Crystal structure of TOG1-TOG2 arrays in the recruitment state conformation (TOG square assembly) with interfaces 1 and 2 (marked by arrows) stabilizing this conformation (Nithianantham *et al.*, 2018). (B) Crystal structure of the polymerization state showing an unfurled array, with TOG1 lies base and TOG2 positioned above, while bound to two αβ-tubulins polymerized head-to-tail (Nithianantham *et al.*, 2018).

are monomers (Al-Bassam and Chang, 2011). TOG3 and TOG4 in the metazoan orthologues are exclusively related to TOG1 and TOG2, respectively, leading these metazoan proteins to be considered internal dimers with tandem TOG1-TOG2 and TOG3-TOG4 arrays separated by a positively charged SK-rich-like region (Brouhard *et al.*, 2008; Al-Bassam and Chang, 2011; Widlund *et al.*, 2011). TOG domains selectively bind curved αβ-tubulin conformations found in solution and at the extreme tip of MT plus ends. On αβ-tubulins adopting a straight conformation during MT polymerization, TOG domains are presumed to lose affinity for the newly incorporated tubulin. This feature is termed catch and release and it may explain how TOG domains bind and release αβ-tubulins during MT polymerase activity (Ayaz *et al.*, 2012, 2014; Brouhard and Rice, 2014). It remains unknown how this catch and release feature of TOG domains may function during MT polymerization and what specific roles maybe served by TOG1 and TOG2 in arrays during MT polymerase and plus-end tracking functions.

XMAP215, Stu2, and Alp14 proteins are capable of tracking the extreme tips of polymerizing MT plus ends without any additional factors as demonstrated by in vitro studies, suggesting conservation of this feature across species (Brouhard *et al.*, 2008; Al-Bassam *et al.*, 2012). Single XMAP215 molecules reside at dynamic MT plus ends for several seconds where they polymerize multiple αβ-tubulins and translocate with the polymerizing MT ends prior to dissociating (Brouhard *et al.*, 2008; Al-Bassam *et al.*, 2012). This form of plus-end tracking is distinct from that of EB1 proteins, which bind to extended MT lattice zones near MT plus ends defined by GTP or GDP-Pi polymerized αβ-tubulin states (Asbury, 2008; Brouhard *et al.*, 2008; Akhmanova and Steinmetz, 2011, 2015). EB1 proteins dissociate when MT plus ends transition to the GDP state, leading to a comet-like treadmilling form of tracking (Maurer *et al.*, 2011, 2014). In contrast, many studies implicate XMAP215's TOG domains and SK-rich regions in MT polymerase and plus-end tracking. However, the specific functions of TOG1 and TOG2 domains or their array organization for processive MT plus-end tracking remain unknown (Brouhard *et al.*, 2008; Widlund *et al.*, 2011; Al-Bassam *et al.*, 2012). Despite extensive study, we lack a mechanistic understanding for how MT polymerases accelerate MT polymerization while simultaneously processively tracking MT plus ends is still lacking.

We recently described a polarized unfurling MT polymerase model based on structural and biochemical studies to explain how assemblies of TOG arrays act as MT polymerases that accelerate αβ-tubulin assembly while tracking MT plus ends (Nithianantham *et al.*, 2018). TOG1-TOG2 arrays were observed in two conformations: 1) a recruitment state in which dimeric TOG1-TOG2 arrays form a square-like organization while recruiting four unpolymerized αβ-tubulins (Figure 1A). This complex is stabilized by two sets of interfaces (termed interfaces 1 and 2) present along the short edges of each TOG domain; 2) a polymerization state in which a single TOG1-TOG2 array becomes unfurled into an extended conformation and is bound to two αβ-tubulins that are polymerized head-to-tail into a curved protofilament (Figure 1B). On the basis of this organization, we postulate that TOG1 binds the αβ-tubulin closest to the fully assembled MT plus end, whereas TOG2 binds the αβ-tubulin at the extreme end of the newly assembled protofilament. The model, which suggests an unfurling of TOG1-TOG2 arrays from the recruitment state to the polymerization state, is promoted by steric hindrance as a result of docking of the TOG square onto MT plus ends via TOG1-αβ-tubulin, but not when the TOG square docks via TOG2-αβ-tubulin (Nithianantham *et al.*, 2018). The model suggests that the TOG square assembly forms in solution prior to MT plus-end docking and inhibits premature polymerization. Thus, we predict that the TOG square assembly is important for both MT plus-end tracking and polymerase, whereas αβ-tubulins recruitment by TOG1 and TOG2 may influence those two functions uniquely.

Here, we describe the roles for αβ-tubulin recruitment and self-assembly of yeast TOG arrays in the processive MT plus-end tracking and MT polymerase functions. We study two classes of Alp14 mutants, which were previously biochemically and structurally characterized (Nithianantham *et al.*, 2018), using a combination of in vivo live imaging of mutants with dynamic MTs in *Schizosaccharomyces pombe* cells and in vitro reconstitution of these mutants with dynamic MTs using total internal reflection (TIRF) microscopy. These approaches allow us to describe distinct defects exhibited by these mutants in MT polymerization and MT plus-end tracking. We show that αβ-tubulin recruitment by TOG1 and TOG2 serves concerted, but specific, functions in the MT polymerase and MT plus-end tracking activities. TOG1 is more critical for processive MT plus-end tracking, whereas TOG2 is more integral for accelerating αβ-tubulin polymerization. Inactivating the TOG square assembly interfaces leads to defects in processive MT plus-end tracking and proportional defects in accelerating αβ-tubulin polymerization. Our studies reveal a functional separation between plus-end tracking and αβ-tubulin polymerization accelerating features, allowing us to assign discrete function to elements within TOG arrays. These data lead to conclusions that validate and reinforce the polarized unfurling model (Nithianantham *et al.*, 2018). Our studies suggest that a dynamic cycle between the recruitment and polymerization promote the conserved MT polymerase and plus-end tracking functions.

RESULTS

TOG1 and TOG2 exhibit specific contribution to persistent MT plus-end tracking and MT polymerase functions in vivo

Alp14 consists of a TOG1-TOG2 array, a SK-rich region, and a dimerizing coiled-coil (Supplemental Figure S1A) (Al-Bassam *et al.*, 2012). To determine the roles for the αβ-tubulins recruited by TOG1 and TOG2 in MT polymerase and plus-end tracking activities, we studied Alp14 mutants in which we inactivated αβ-tubulin binding interfaces in TOG1,TOG2 and both by introducing point mutations in their αβ-tubulin binding loops (Supplemental Figure S1, A and B) (Nithianantham *et al.*, 2018). We previously studied these three Alp14 mutants, TOG1M, TOG2M and TOG1+2M, and characterized their biochemical activities. TOG1M dimer contains two active TOG2 domains and it exchanges αβ-tubulin rapidly. TOG2M dimer contains two active TOG1 domains and binds αβ-tubulin tightly. TOG1+2M does not bind αβ-tubulin (Al-Bassam *et al.*, 2012; Nithianantham *et al.*, 2018). We introduced these *alp14* mutants into *S. pombe* using homologous recombination and confirmed their replacement of the native chromosomal *alp14*+ gene copies.

First, we analyzed viability of the wild-type, TOG1M, TOG2M, and TOG1+2M mutant *S. pombe* strains using a spot yeast colony growth assay under the effect of temperature and MT-depolymerizing drugs. The *alp14*Δ cells are sensitive to growth in cold (20°C) and high (36°C) temperatures (Garcia *et al.*, 2001) and to the presence of the MT inhibitor methyl 2-benzimidazolecarbamate (MBC) (Sato *et al.*, 2004; Sato and Toda, 2007). TOG1+2M cells showed a very similar growth defect to *alp14*Δ cells (Supplemental Figure S1C). Surprisingly, TOG1M cells showed little growth defect with or without MBC at 20–36°C (Supplemental Figure S1C). In contrast, TOG2M cells displayed a more severe growth defect, which was intermediate between wild-type and TOG1+2M cell phenotypes at 20–36°C (Supplemental Figure S1C).

Next, we used live-cell imaging to visualize wild-type or mutant Alp14, which are C-terminally fused to green fluorescent protein (GFP), while tracking the plus-ends of dynamic MTs, visualized using mCherry α-tubulin. To our knowledge, our study is the first to utilize live-cell imaging to quantitatively analyze MT plus-end and polymerase defects in relation to biochemically characterized Alp14 mutants, even though Alp14 functions in interphase and mitosis were studied previously (Al-Bassam *et al.*, 2012; Kakui *et al.*, 2013; Okada *et al.*, 2014; Flor-Parra *et al.*, 2018). Fields, shown in Supplemental Figure S1D, reveal dynamic MTs with Alp14-GFP decorating their plus-ends in wild-type and TOG-inactivated strains. Time-lapse imaging shows that Alp14 tracks dynamic MT plus ends as they polymerize toward the cell cortex emanating from the central bundles allowing measuring polymerization rates and tracking patterns (Figure 2B; for details on approach, see Supplemental Figure S2).

The MT polymerization rates in *alp14*Δ cells (1.1 μm/min) were threefold lower than in wild-type cells (3.18 ± 0.85 μm/min), confirming that Alp14 expression only accelerates MT polymerization threefold at maximum, as shown previously (Al-Bassam *et al.*, 2012) (Supplemental Table S3; Figure 2C). MT polymerization rates decreased significantly in the TOG1M and TOG2M strains (1.55 ± 0.48 and 1.32 ± 0.31 μm/min, respectively), whereas the TOG1+2M strain exhibited the most severe MT polymerization rate decrease, similar to *alp14*Δ cells (1.15 ± 0.25 μm/min). These data are in contrast to previous work showing only a small MT growth defect in Alp14-ΔTOG1 strain (Flor-Parra *et al.*, 2018); a possible reason for the difference in severity is that TOG1 deletion generates a gain-of-function in Alp14 while TOG1 mutant inactivation does not. The TOG-inactivated mutants also exhibited clear MT shrinkage defects (Al-Bassam *et al.*, 2012). The pattern of defects in MT shrinkage was similar to those observed for MT polymerization defects (Supplemental Figure S3C). Compared to wild type, TOG1M was less severe, whereas TOG2M and TOG1+2M had the most severe defects and was similar to *alp14*Δ (Supplemental Table S2 and Supplemental Figure S3C). These findings indicate that TOG2 domain may play a larger role than TOG1 in both MT polymerization and depolymerization.

Live imaging reveals some TOG-inactivated mutants exhibit defects in the persistence of tracking dynamic MT plus ends in vivo. Plus-end tracking persistence is defined as Alp14's ability to remain at the MT plus end during the entire MT growth phase. In wild-type cells, Alp14-GFP tracked polymerizing MT plus ends throughout growth phases, producing smooth tracks with consistent intensity throughout (Figure 2B, left panel). In contrast, TOG1M and TOG1+2M strains showed large variations in Alp14 intensity at MT plus ends, with sudden drops in intensity during growth phases (Figure 2D; Supplemental Table S3). This loss of persistent high intensity tracking signal is observed for TOG1M and TOG1+2M. Each dynamic MT plus end analyzed remained in focus, suggesting the MT end remained at a similar Z-height during imaging, whereas the Alp14 signal dropped (arrows in Figure 2B; additional example kymographs in Supplemental Figure S3A). Surprisingly, Alp14-GFP tracks in the TOG2M strain were smooth with little change in intensity at MT plus ends, similar to the wild-type strain, although the Alp14 signal intensity is slightly dimmer than those in wild-type cells (Figure 2, B and D; see additional examples in Supplemental Figure S3A). Roughly 71% of MTs in TOG1M (n = 55) and 90% in TOG1+2M mutants (n = 14) exhibited some abnormality in maintaining Alp14 intensity at MT plus ends, whereas only 38% of MT in TOG1M exhibited abnormal tracks. Only 18% of MTs observed in wild-type cells exhibited abnormal tracks (Figure 2D; Supplemental Figure S3D).

Next, we quantitated changes in Alp14-GFP persistence in MT plus-end tracking in these strains by calculating tracking ratios for Alp14-GFP signal at growing MT plus ends. The tracking ratio is a measure of Alp14 persistence at MT plus ends and is defined as the ratio of the duration of Alp14 signal that is above background divided by the duration of MT polymerization for that event (Supplemental Figures S2 and S4, A and B; Supplemental Materials and Methods). A high tracking ratio indicates a highly persistent plus-end tracking signal that follows MT plus end throughout polymerization, whereas a low ratio indicates decreased persistence in tracking MT plus ends, with tracking signal disappearing part of the way through the MT polymerization phases. In each strain, durations for Alp14-GFP tracking and the corresponding MT plus-end polymerization all showed Gaussian distributions (Supplemental Figure S4, A and B). Tracking ratio plots show that in wild-type cells, Alp14 exhibits a high tracking ratio with low variance (average 0.98; range 18.7%). In the TOG1M strain, the tracking ratio decreased by 15% and exhibited high variance (Figure 2F; average 0.84; range 87.0%). In contrast, TOG2M strain showed a nearly identical tracking ratio to the wild-type strain, which was also matched by its low variance (TOG2M: average 0.96; range 18.7%). We observed a very low tracking ratio with extremely high variance in TOG1+2M cells (Figure 2F: average 0.56; range 100%), and tracking defects were observed in almost every MT measured in that strain (Figure 2B).

Measuring maximal MT length distribution emanating from the central bundle in vivo in also revealed a similar pattern of functional defects (Supplemental Figure S3B). We determined the proportion of MTs reaching the cell cortex prior to undergoing catastrophe events (Supplemental Figure S3D). In TOG1M, TOG2M and TOG1+2M cells, MT bundles were short and had few MTs reach the

cell cortex compared with those in wild-type cells. However, the TOG1M defect was weaker compared with the TOG2M defect. These data indicate that αβ-tubulin recruitment by both TOG1 and TOG2 domains is required for optimal Alp14 activity, but these activities have unique contributions to either the MT polymerase or the MT plus-end tracking functions. The αβ-tubulins recruited by TOG1 and TOG2 both contribute to MT plus-end tracking and MT polymerase functions in vivo. However, TOG1 has a larger role in persistent MT plus-end tracking, whereas TOG2 is crucial for proper MT polymerase function.

TOG2 αβ-tubulin binding plays a more critical role than TOG1 in MT polymerase activity in vitro

To understand the molecular basis for TOG-inactivation defects, we purified recombinant Alp14 that is C-terminally fused to mNeonGreen (mNG) (residues 1–690; termed wt-Alp14) and matching versions of the TOG inactivated mutants. (Supplemental Figure S1A) (Al-Bassam *et al.*, 2012). We reconstituted wt-Alp14 and TOG-inactivated mutants using dynamic MT polymerization assays visualized by TIRF microscopy (as shown in Supplemental Figure S5C). Our previous biochemical analyses indicate that TOG1 and TOG2 domains differ in αβ-tubulin binding affinities and release rates by more than twofold (Figure 3A) (Nithianantham *et al.*, 2018). We have previously shown that the affinity of each TOG domain for αβ-tubulin can also be modulated by increasing the solution ionic strength. These affinities increase 20-fold when the solution's ionic strength is decreased from 200 to 50 mM KCl (Figure 3A) (Nithianantham *et al.*, 2018). Our previous analysis indicates that at 8 μM soluble αβ-tubulin and 1 μM wt-Alp14 concentrations, TOG1 domains bind αβ-tubulin tightly at both 50 mM and 200 mM KCl. TOG2 domains bind to αβ-tubulin tightly at 50 mM KCl and loosely at 200 mM KCl, where the αβ-tubulin is rapidly released (Nithianantham *et al.*, 2018) (Figure 3A).

First, we determined how change in affinities of TOG1 and TOG2 for αβ-tubulin due to the decrease in ionic strength (200–50 mM KCl) influences Alp14 MT polymerase activity. In the absence of Alp14, MT plus-end polymerization rates at 50 mM KCl slightly increased compared with that of 200 mM KCl (0.38 μm/min at 200 mM KCl and 0.50 μm/min at 50 mM KCl; Supplemental Table S1). Increasing the concentration of wt-Alp14 accelerated MT plus-end polymerization rates by roughly threefold at 200 mM KCl (0.38 μm/min to a maximal 1.52 μm/min). Alp14 tightly tracked MT plus ends with a dim intensity signal, as shown previously (Al-Bassam *et al.*, 2012). At 50 mM KCl, increasing the wt-Alp14 concentration induced a weaker MT polymerase activity which plateaus at ~1.07 μm/min. This indicates an ~40% decrease in activity at 50 mM KCl compared with 200 mM KCl, suggesting that when both TOG1 and TOG2 domains' affinities are enhanced by 20-fold and the αβ-tubulin release rates are reduced, wt-Alp14 is unable to fully accelerate MT polymerization. This supports the idea that the rapid release of αβ-tubulin by TOG2 is critical for maximal MT polymerase activity.

Next, we studied the effect of TOG-inactivation and salt concentration on MT polymerase activity (Figure 3, B and C; Supplemental Figure S5E) (Nithianantham *et al.*, 2018). At 200 mM KCl, TOG1M and TOG2M show distinct defects in MT polymerase. TOG1M and TOG2M exhibit a maximal MT polymerization rate of 0.84 and 0.70 μm/min, respectively, indicating a 44% decrease for TOG1M and a 54% decrease for TOG2M compared with wt-Alp14 (Figure 3, B and C; Supplemental Movie S1). Surprisingly, the maximal MT polymerase for TOG2M was nearly indistinguishable from that of TOG1+2M (~0.65 μm/min) (Figure 3, B and C; Supplemental Movie S1), suggesting that the SK-rich region in the Alp14 sequence plays a role in MT polymerase activity, as noted by a recent study (Geyer *et al.*, 2018). However, at 50 mM KCl, where the αβ-tubulin release from TOG domains is made 20-fold slower, TOG1M showed an ~40% decrease in MT polymerase activity (0.74 μm/min), whereas TOG2M showed an ~83% decrease (0.38 μm/min) compared with wt-Alp14 (1.07 μm/min) (Figure 3, D and E). At 50 mM KCl, the TOG2M-aided MT polymerization rate is slower than the MT polymerization without Alp14 (0.50 μm/min), indicating that the high affinity of TOG1 for αβ-tubulin likely inhibits αβ-tubulin polymerization in the absence of an active TOG2. TOG1M and TOG2M MT shrinkage rates at 50 mM KCl were also dramatically decreased in a similar pattern (Figure 3D). These data correlate the critical role for αβ-tubulin release by TOG1 and TOG2 to their role in MT polymerase activity, a feature termed catch and release and hypothesized by Ayaz *et al.* (2012). These findings indicate that αβ-tubulin recruitment by TOG1 and TOG2 contribute to a concerted function, yet serve unequal roles in MT polymerase. TOG2 plays a larger role than TOG1 in MT polymerase activity. This unequal contribution further diverges at 50 mM KCl, where the αβ-tubulin binding affinities of TOG1 and TOG2 are further enhanced.

TOG1 binding to αβ-tubulin plays a more critical role than TOG2 in MT plus-end tracking in vitro

We next sought to understand the MT plus-end tracking patterns for wt-Alp14 and TOG-inactivated mutants in the two ionic strength conditions (50 and 200 mM KC). Our analyses indicated that TOG1M exhibited a more severe defect than TOG2M, which matched the tracking efficiency of wt-Alp14 (Figure 3E; Supplemental Movie S1). At 50 and 200 mM KCl, wt-Alp14 tightly tracked polymerizing MTs with a dim tip-tracking signal as seen previously (Al-Bassam *et al.*, 2012). Almost all polymerizing MT ends retained wt-Alp14 tracking signals throughout polymerizing phases (Figure 3C; Supplemental Figure S5E; Supplemental Movie S1). At 200 mM KCl, TOG1M exhibited mostly short tracks and extensive periods without tracking (Figure 3C, second panel; Supplemental Movie S1). At 50 mM KCl, TOG1M exhibited long tracks accompanied by random dissociation from MT plus ends, followed by diffusion along MT lattices (Figure 3E, left and third panels). The MT lattice-diffusing TOG1M molecules often rebind and track the depolymerizing MT plus ends (Figure 3E, second panel). On the other hand, TOG2M tracked MT plus ends throughout polymerizing phases, similar to wt-Alp14 at both 50 and 200 mM KCl (Figure 3, C and D; Supplemental Movie S1). TOG1+2M did not bind polymerizing MT plus ends at 200 mM KCl and mostly bound along MT lattices. For this reason, we did not study MT plus-end tracking for TOG1+2M any further in vitro (Figure 3C, fourth panel). The potent MT lattice-binding exhibited by TOG1+2M indicates that the SK-rich region dominates localization in the absence of active TOG domains, matching observations made for a similar mutant for the protein Stu2 (Geyer *et al.*, 2018). The MT plus-end tracking activities of TOG1M and TOG2M are fundamentally different beyond the differences in the TOG1 and TOG2 αβ-tubulin binding affinities. Despite the similarly high affinities of TOG1 and TOG2 for αβ-tubulin at 50 mM KCl (Nithianantham *et al.*, 2018), our data clearly indicate these two TOG domains serve concerted roles in MT plus-end tracking with TOG1 binding to αβ-tubulin being vital for efficient tracking.

Processive tracking at MT plus ends requires TOG1-αβ-tubulin binding

Quantitative analyses of MT plus-end tracking features revealed that TOG2M and wt-Alp14 MT plus-end tracking is nearly identical,

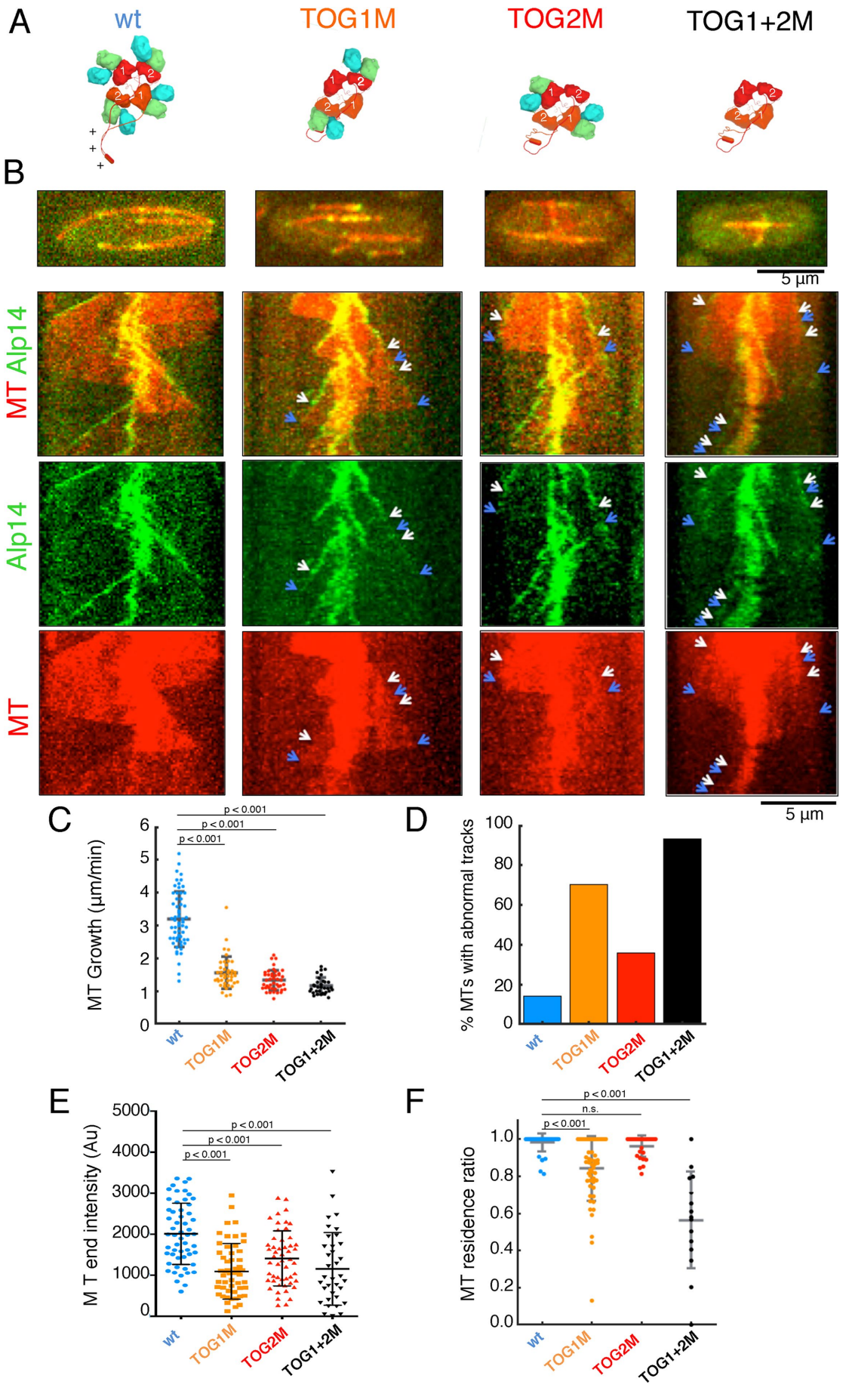
A
wt
TOG1M
TOG2M
TOG1+2M
B
5 µm
MT Alp14
Alp14
MT
5 µm
C
MT Growth (µm/min)
p < 0.001
p < 0.001
p < 0.001
wt
TOG1M
TOG2M
TOG1+2M
D
% MTs with abnormal tracks
wt
TOG1M
TOG2M
TOG1+2M
E
M T end intensity (Au)
p < 0.001
p < 0.001
p < 0.001
wt
TOG1M
TOG2M
TOG1+2M
F
MT residence ratio
p < 0.001
n.s.
p < 0.001
wt
TOG1M
TOG2M
TOG1+2M

whereas TOG1M tracking is severely compromised. We analyzed the wt-Alp14, TOG1M, and TOG2M signal intensities and tracking duration and calculated a MT plus-end tracking ratio at saturating (200 nM) concentrations at 200 mM KCl (see *Materials and Methods*). For each MT growth event, an automated algorithm was used to measure the Alp14 MT plus-end fluorescence intensity, duration of tracking, and MT polymerization duration (Supplemental Figure S6A; *Materials and Methods*). The Alp14 tracking intensities, durations, and MT polymerization durations all fitted to Gaussian distributions (Supplemental Figure S7). The wt-Alp14 and TOG2M exhibited a single average plus-end tracking intensity with a tight distribution (Supplemental Figure S7C). In contrast, TOG1M showed a bimodal intensity distribution with a roughly twofold difference between the two average values and the higher intensity matching those of wt-Alp14 and TOG2M. The tracking ratio analyses suggest that inactivation of TOG1 leads to defects in cooperativity among Alp14 molecules in attaching to MT plus ends, producing two occupancy levels, presumed at ~100% and ~50%, whereas TOG2 inactivation leads to nearly constant ~100% occupancy similar to that for wt-Alp14 (Supplemental Figure S7C). The average tracking time for TOG1M decreased by ~30% compared with TOG2M and wt-Alp14 (95.2 s compared with 125.3 s) (Supplemental Figure S7D). To globally compare the varied tracking durations and corresponding MT polymerizing phases, we determined tracking ratios for wt-Alp14, TOG1M, and TOG2M, as previously described (Figure 4, A and B; details shown in Supplemental Figure S7; *Materials and Methods*). Tracking ratio patterns revealed that wt-Alp14 and TOG2M exhibit a very high tracking ratio with fairly low variance (wt-Alp14: 0.89 average; range 36.9%; TOG2M 0.91 average; range 40%; no significant difference with wt-Alp14; Figure 4B). In contrast, TOG1M exhibited a 17% decrease in average tracking ratio and showed high variance (0.72 average; range 86.13%; Figure 4B). Thus, in contrast to wt-Alp14 and TOG2M, TOG1M molecules appeared to be asynchronous in tracking MT plus ends, exhibiting defects in cooperativity that lead to short tracks with high variance. These data reinforced the critical role for TOG1 in efficient MT plus-end tracking, whereas TOG2 has a minor role in MT plus-end tracking, despite its importance in MT polymerase activity.

To further characterize plus-end tracking, we utilized a single-molecule Alp14 dynamic MT TIRF assay to measure the average dwell time of single Alp14 molecules at growing MT plus ends. To avoid premature photobleaching, we used a C-terminal-SNAPf-tagged Alp14 (herein termed Alp14-SNAP) on which a SNAP-surface Atto-488 fluorophore is covalently attached (Supplemental Figures S5, A and B, and S8; see *Materials and Methods*). We spiked 5–10 nM Atto 488-labeled Alp14-SNAP into 190–195 nM nonlabeled Alp14-SNAP to visualize the binding and dissociation of single Alp14 molecules at MT plus ends (Supplemental Figure S8A). At such conditions, few fluorescent Alp14-SNAP-Atto 488 molecules were observed to bind to polymerizing MT plus ends (Supplemental Figure S8). A bimodal intensity distribution confirmed these events represent individual Alp14 dimers with either one or both SNAP tags in the Alp14 dimers being labeled with Atto 488 dye (Supplemental Figure S8B). We also measured photobleaching profiles for the Alp14-SNAP-labeled Atto-488 and confirmed that the fluorophore half-life lasts twice as long as the average duration of the MT polymerizing phase (Supplemental Figure S8B), supporting the notion that Alp14-SNAP-Atto-488 is more suitable than Alp14-NG for long, high-frame-rate movies (Supplemental Figure S8B). Dwell times of 100–150 events of wt-Alp1, TOG1M, and TOG2M were used to assemble frequency distributions that were fitted to a exponential decay function (Figure 4C; see *Materials and Methods*). We measured a mean dwell time of 129.3 s ($n = 164$) for wt-Alp14 at polymerizing MT plus ends, suggesting Alp14 is an extremely processive tracking protein (Figure 4C; additional example kymographs are shown in Supplemental Figure S8C; Supplemental Movie S2). At this dwell time, Alp14 is 20-fold more processive in tracking MT plus ends than the dwell times reported for XMAP215 and Stu2 (Brouhard *et al.*, 2008; Geyer *et al.*, 2018). A potential explanation for this major difference may be attributed to the rapid photobleaching of GFP-fused Stu2 and XMAP215 proteins leading to a severe underestimation in the dwell times for these proteins in those studies, whereas our study utilized a stable Atto-488 chemical dye, which resists photobleaching (Brouhard *et al.*, 2008; Geyer *et al.*, 2018). To ensure the accuracy of our analyses, we also collected data at a higher frame rate (~0.5 s/frame) and calculated similar dwell times for wt-Alp14, confirming that the longer frame rate

FIGURE 2: The αβ-tubulins recruited by TOG1 and TOG2 serve distinct roles in MT plus-end tracking and MT polymerase in vivo. (A) Right, Scheme for the αβ-tubulin binding and release activities by wt-Alp14, which forms a TOG square organization. Middle and left panels show the defects αβ-tubulin recruitment by TOG1M, TOG2M, and TOG1+2M mutants, summarized based on published studies (Nithianantham *et al.*, 2018). (B) *S. pombe* cells expressing wt-Alp14, TOG1M, TOG2M, and TOG1+2M mutants. Top, raw cell images with MTs marked with mCherry-Atb2 tubulin (red) and Alp14-GFP (green). Bottom, kymographs of dynamic MTs and Alp14-GFP. wt-Alp14 tracks MT plus ends. TOG1M, TOG2M, and TOG1+2M all track the plus ends of dynamic MTs. White arrows, beginnings of abnormal MT polymerization events; blue arrows, ends of such events. Additional example kymographs are shown in Supplemental Figure S3A. (C) MT polymerization rate spreads and averages for wt cells, TOG1M, TOG2M, and TOG1+2M cells highlighting the function of TOG domains in MT polymerization (Supplemental Table S3). TOG2M is similar to that of TOG1+2M, whereas TOG1M is a slightly higher MT growth rate. MT lengths and shrinkage rates are shown in Supplemental Figure S3C. *t* Tests were performed to compare the control to each condition. The *p* value is reported for each comparison marked. Error bars represent SD of the condition. (D) Proportion of dynamic MTs with abnormal tracking in each strain. TOG1M, and TOG1+2M show progressively higher proportions of these events than wt cells, whereas TOG2M strain shows lower proportions. (E) Distribution and average of Alp14-GFP intensities at growing MT plus ends in each strain. *t* Tests were performed to compare the control to each condition. The *p* value is reported for each comparison marked. Error bars represent SD of the condition. (F) MT plus-end tracking ratios of Alp14 signal at dynamic MTs describing persistence in plus-end tracking. wt-Alp14 and TOG2M are associated with high tracking ratios with low variance (80–100%), whereas TOG1 has lower MT tracking ratio and high variance (10–70%) and TOG1+2M has the lowest plus-end tracking ratios and extremely high variance (10–60%). Average and variance of values are reported in Supplemental Table S1. *t* Tests were performed to compare the control to each condition. The *p* value is reported for each comparison marked. ns, indicates no statistical difference observed. Error bars represent SD of the condition.

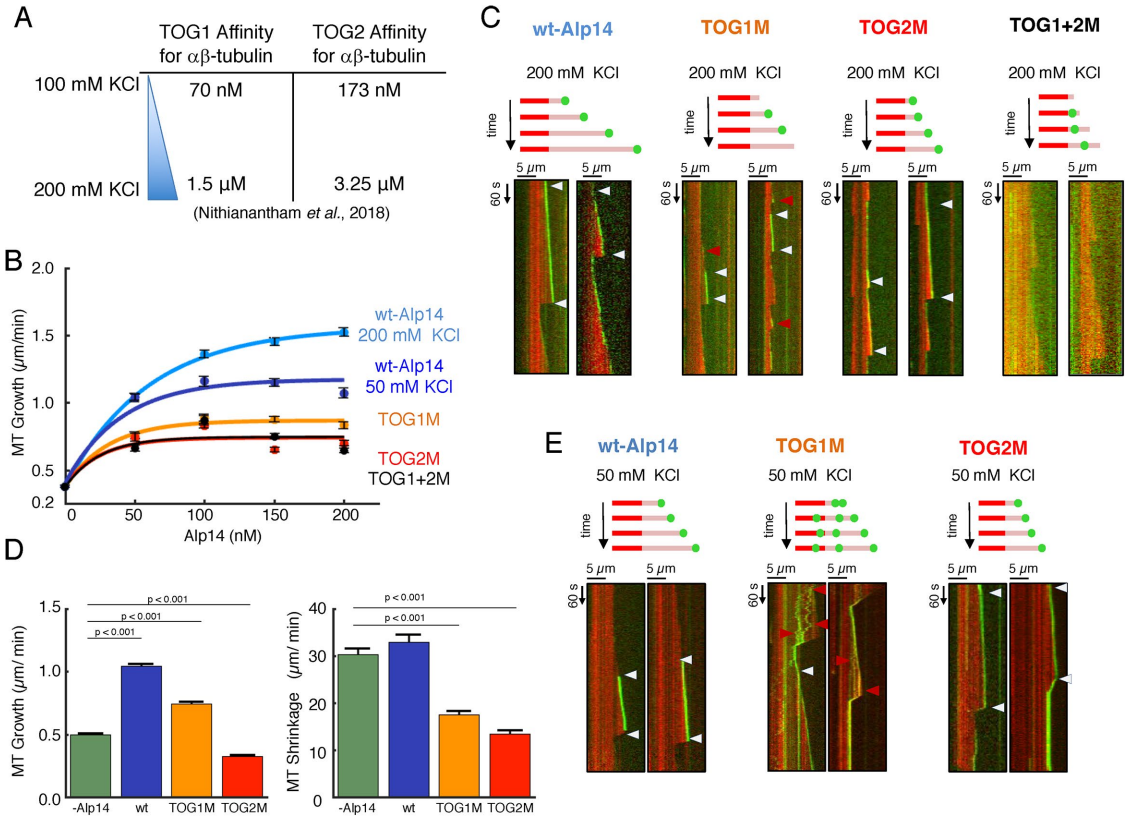

FIGURE 3: The αβ-tubulin recruited by TOG1 and TOG2 serve concerted but unique roles MT polymerase and plus-end tracking. (A) TOG domain affinities for tubulin dimers measured by isothermal titration calorimetry (ITC) at 100 and 200 mM KCl (Nithianantham *et al.*, 2018). (B) Average MT dynamic polymerization rates for various Alp14 constructs and concentrations. Values are reported in Supplemental Table S1. The curves were fitted using the exponential function a-b*e(-c*x). Error bars represent the SEM of each point. (C) Top, schematic for MT dynamic polymerization and Alp14 localization at 200 mM KCl; bottom, kymographs of individual dynamic MTs with wt-Alp14 or mutants at 200 mM KCl. White arrows denote beginning and the end of each tracking events, and red arrows denote rapid binding and dissociation events. (D) Average MT polymerization and shrinkage rates of dynamic MTs in the absence (-Alp14) or the presence of 50 nM wt-Alp14, TOG1M, and TOG2M mutants at 50 mM KCl, revealing the unequal contributions of TOG1 and TOG2. *t* Tests were performed to compare the control to each condition, and the *p* value is reported for each comparison marked. Error bars represent SD of the condition. Error bars represent SEM of the condition. (E) Model for observed MT polymerization activity and Alp14 localization at 50 mM KCl; bottom, kymographs of individual dynamic MTs with wt-Alp14 or mutants at 50 mM KCl. White arrows denote beginning and end of tracking events, and red arrows denote diffusion along MT lattices in TOG2M.

imaging observed single events and did not involve multiple association and dissociation events (unpublished data). TOG1M molecules showed an average dwell time of 57.4 s (n = 130), which was ~43% of that for wt-Alp14 (Figure 4C; additional example kymographs are shown in Supplemental Figure S8D; Supplemental Movie S2). TOG2M exhibited an average dwell time of 132.2 s (n = 152) at MT plus ends, which is indistinguishable from wt-Alp14 (Figure 4C; additional example kymographs are in Supplemental Figure S8E; Supplemental Movie S2). Thus, at the single molecule level, TOG1M resides at MT plus ends for 57% less time compared with wt-Alp14 or TOG2M. This is consistent with the defects observed in MT plus-end tracking ratios in bulk dynamic MT assays (Figure 4, A and B).

Using dwell times and MT polymerization rates coupled with the assumption that 13 Alp14 molecules bind to 13-protofilament MTs, we calculated the number of αβ-tubulins added per MT plus end or protofilament in each Alp14 dimer binding event, as described in Supplemental Table S2. The wt-Alp14 polymerizes ~422 αβ-tubulins per event, TOG1M polymerizes ~99 αβ-tubulins per event, whereas TOG2M polymerizes ~193 αβ-tubulins per event. Although the TOG2M polymerization rate is slower than that of TOG1M, it remains bound for twice as long, leading to twofold more αβ-tubulin polymerized. Thus, within the homodimeric Alp14, TOG1 and TOG2 contribute to both MT plus-end tracking and MT polymerase; however, our data clearly reveal that TOG1 contributes more to processive tracking, whereas TOG2 is crucial for MT polymerase function.

Square assembly interfaces are important for MT polymerase and plus-end tracking in vivo

The polarized unfurling model predicts that the TOG square assembly is a recruitment state and is stabilized by sets of interfaces (Figure 1) (Nithianantham *et al.*, 2018). We predict that disruption of the interfaces stabilizing this intermediate would lead to defects in both MT polymerization and plus-end tracking functions (Nithianantham *et al.*, 2018). Thus, we studied three Alp14 mutants that specifically disrupt either or both interfaces 1 and 2 (Nithianantham *et al.*, 2018) (Figure 5A; Supplemental Figure S9, A and B). We studied an eight-residue mutant that disrupts interface 1, which stabilizes the interdimer TOG array assembly, termed INT1. The second mutant studied was a seven-residue mutant designed

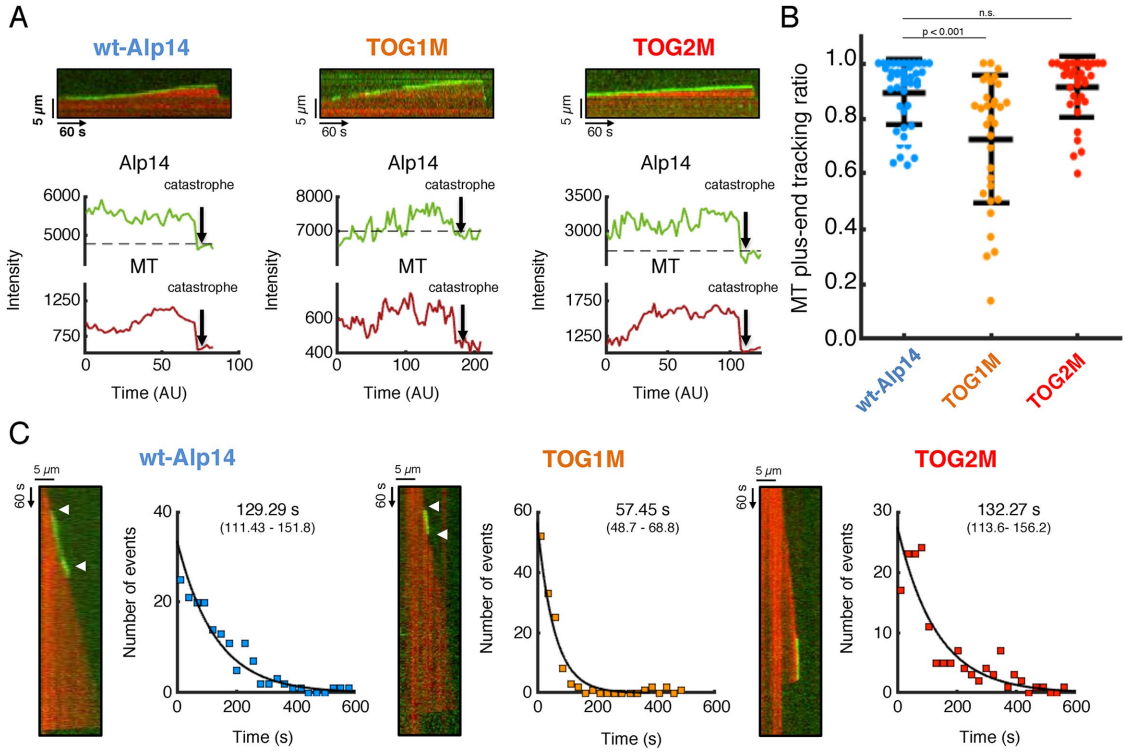

FIGURE 4: TOG1 is critical for processive MT plus-end tracking. (A) Measuring tracking ratios for wt Alp14, TOG1M, and TOG2M at growing MT plus ends. Top, horizontal kymograph; middle, Alp14 plus-end tracking intensity (green trace) compared with background (broken line); bottom, MT intensity (red trace) at the plus end during the polymerizing phase until catastrophe (arrow) compared with background (broken line). wt-Alp14 and TOG2M signal persists at MT plus ends throughout, whereas TOG1M shows short zones with little or no signal, denoted by a decrease below background. Additional examples are found in Supplemental Figure S6, B–D. (B) Averages and distributions of tracking ratios for wt-Alp14, TOG1M, and TOG2M. This a result of detailed analysis described in Supplemental Figure S7. *t* Tests were performed to compare the control to each condition, and the *p* value is reported for each comparison marked. Error bars represent SD of the condition. (C) Single-molecule dynamic MT polymerization reveals the mean dwell time for wt-Alp14, TOG1M, and TOG2M. Left, example kymographs with single molecule localization at MT plus ends, Right, dwell time frequencies, and fits to an exponential decay model. Details of these single-molecule experiments and additional examples are presented in Supplemental Figure S8.

to disrupt interface 2, stabilizing the intradimer TOG1 and TOG2 orientation within a single array, termed INT2 from herein. INT1 and INT2 mutations were combined in a 15-residue mutant that destabilizes both interfaces 1 and 2, termed INT1+2 (Supplemental Figure S9, A and B) (Nithianantham *et al.*, 2018). We have previously shown that INT1, INT2, and INT1+2 recruit four αβ-tubulins at low ionic strength and release two αβ-tubulins at 200 mM KCl, identical to that of wt-Alp14 (Nithianantham *et al.*, 2018). However, negative stain electron microscopy revealed that INT1 and INT2 did not form normal αβ-tubulin bound TOG square organization but instead formed cornerlike complexes or unfurled polymerized αβ-tubulins, whereas INT1+2 exhibited necklace-like assemblies without any organized assemblies (Nithianantham *et al.*, 2018) (summarized in Figure 5A). Mutants with fewer residues showed substantial square assembly activity due to partially active interfaces (unpublished data). Thus, INT1, INT2, and INT1+2 mutants are described here, which included 7–15 residues and were sufficient to disrupt interfaces 1 and 2 of the square assembly without affecting αβ-tubulin binding.

To determine the physiological roles of square assembly interfaces in vivo, we introduced INT1, INT2, and INT1+2 into the endogenous *alp14*$^{+}$ locus in *S. pombe* cells (Figure 5). Colony growth spot assays did not show defects at the 20–36°C range, nor in the presence of the MT inhibitor MBC (Supplemental Figure S9C). Live-cell imaging of INT-inactivated Alp14-GFP mutants and mCherry-labeled MTs revealed defects in MT polymerization rates (Figure 5C). INT1 and INT2 showed about a 28 and 38% decrease (2.6 ± 0.7 and 2.4 ± 0.6 μm/min, respectively), whereas INT1+2 exhibited a 40% decrease (2.3 ± 0.8 μm/min) compared with wt-Alp14. A similar pattern of defects was observed for MT depolymerization measured in INT1, INT2, and INT1+2 cells (Supplemental Figure S10C), suggesting that inactivating the square assembly affects both MT polymerase and depolymerase activities, similar to the TOG-inactivated mutants.

Imaging Alp14-GFP in the INT mutant strains revealed persistence defects in tracking polymerizing MT plus ends in vivo (Figure 5B; additional example kymographs are shown in Supplemental Figure S10A). In wild-type cells, Alp14-GFP fluorescence intensity remained constant during MT polymerizing phases exhibiting smooth tracking patterns (Figure 5D). In the INT mutant cells, Alp14 intensity at MT plus ends varied extensively, exhibiting signal drop-offs, whereas polymerizing MTs remained in focus (Figure 5D). Close visual inspection of time-lapse image movie frames and/or kymographs revealed defects in persistent tracking of MT plus ends in INT1-, INT2-, and INT1+2-GFP. In these mutants, the signal was observed to suddenly dropp during extensive periods of MT polymerizing phases, despite these MT ends remaining in focus at a constant Z-height (Figure 5B; additional example kymographs are shown in Supplemental Figure S10A). Most tracks displayed uneven

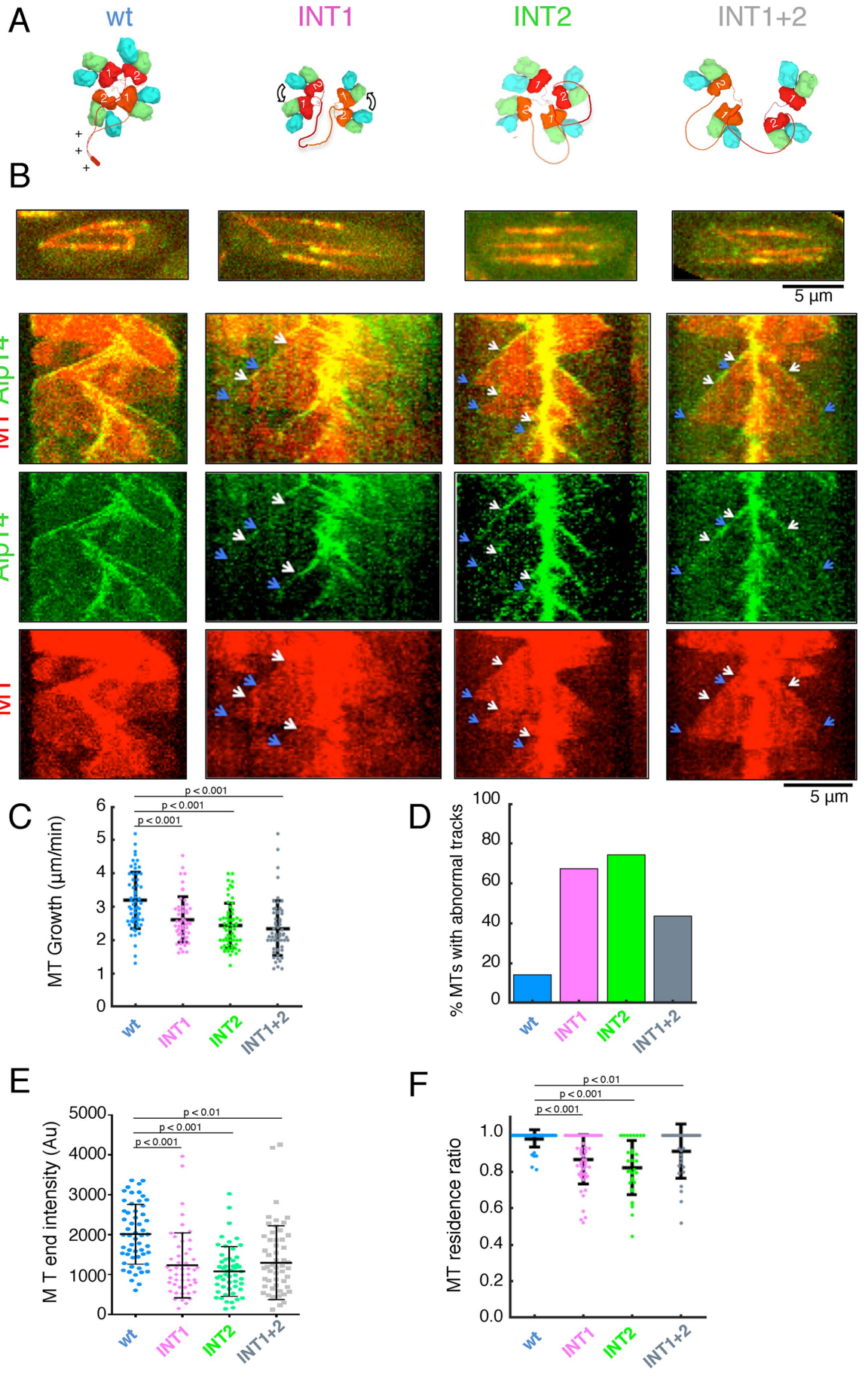
A
wt
INT1
INT2
INT1+2
B
5 µm
MT Alp14
Alp14
MT
5 µm
C
MT Growth (µm/min)
p < 0.001
p < 0.001
p < 0.001
wt
INT1
INT2
INT1+2
D
% MTs with abnormal tracks
wt
INT1
INT2
INT1+2
E
M T end intensity (Au)
p < 0.01
p < 0.001
p < 0.001
wt
INT1
INT2
INT1+2
F
MT residence ratio
p < 0.01
p < 0.001
p < 0.001
wt
INT1
INT2
INT1+2

bright and dim signal intensities (Figure 5B; Supplemental Figure S10A). In INT1 cells, 67% of MTs exhibited abnormal tracking events, while in INT2 cells, 75% of MTs exhibited abnormal tracking events. The INT1+2 mutant exhibited ~43% of MTs with abnormal tracking (Figure 5E).

Measuring the tracking ratios for the INT-inactivated mutants in vivo revealed defects in their processivity at MT plus ends compared with wt-Alp14 (Figure 5F). The binned track durations and MT polymerizing durations showed normal Gaussian distributions (Supplemental Figure S11, A and B). INT1 cells showed a moderate 14% decrease in tracking ratios and exhibited high variance compared with wild-type cells (INT1: average 86.8%; range 47.9%; wild type: average 98.1%; range 18.7%). INT2 showed a 17% decrease in tracking ratio with moderate variance (average: 82.3%; range: 55.4%). INT1+2 cells showed decrease in tracking ratio with moderate variance compared with wild-type cells (average 91.3%; range 48.1%) ($p = 0.001$ for all conditions compared with wt). Next we studied the average lengths of MTs emerging from central bundles in vivo (Supplemental Figure S10B). In INT1, INT2, and INT1+2 cells, MT bundles were short and had fewer MTs reaching the cell cortex than wild-type cells. However, these defects were less severe than in the TOG-inactivated mutant strains. Our in vivo studies suggest that the interfaces stabilizing the square assembly are important for proper MT polymerase activity and MT plus-end tracking. When these interfaces are disrupted, the mutants exhibit defects in persistent plus-end tracking that are directly proportional to their MT polymerase defects (Figure 5).

TOG square assembly interfaces are critical for MT polymerase activity in vitro

To understand the molecular basis for these INT-inactivated mutant defects, we purified recombinant INT1, INT2, and INT1+2 proteins (Supplemental Figure S12), which are C-terminally fused to NG, and tested their MT polymerase activity and plus-end tracking in using MT dynamics TIRF assay as previously described (Supplemental Table S1; Figure 6B). INT1 exhibited a 49.1% decrease in maximal MT polymerase activity (0.96 ± 0.03 μm/min) compared with wt-Alp14, while INT2 displayed a 67.9% loss in maximal MT polymerase (0.75 ± 0.02 μm/min). INT1+2 exhibited the greatest loss in MT polymerase activity (90%) of any Alp14 mutant we have studied thus far in vitro (0.53 ± 0.02 μm/min), which is comparable to the MT polymerization rate without Alp14 (0.38 ± 0.01 μm/min) (Figure 6, B and C; Supplemental Table S1). Thus, despite the ability of these INT-inactivated mutants to bind αβ-tubulins normally in vitro (Nithianantham *et al.*, 2018), INT2 and INT1+2 mutants exhibited defects in MT polymerase activity, whereas INT1 remained partially active.

The INT-inactivated mutants exhibited distinct defects in MT plus-end tracking, which were different from those exhibited by TOG1M (Figure 3C). INT1 displayed repeated cycles of rapid association and dissociation events, each on the order of 10–40 s, while longer MT plus-end tracks were also observed (Figure 6C; Supplemental Movie S3). INT2 exhibited short tracks, similar to TOG1M, and also included rapid association and dissociation cycles, leading to dotted patterns with short tracks (Figure 6C, red arrows; Supplemental Movie S3). INT1+2 exhibited a severe MT plus-end tracking defect in which MT plus-end tracking signal fluctuated on and off with high frequency during MT growth phases, resulting in a highly dotted pattern (Figure 6C; Supplemental Movie S3). These tracking defects indicate that different features in Alp14 were disrupted compared with TOG1M, leading to rapid on and off MT plus-end tracking persistence defects.

TOG square assembly interfaces regulate processive MT plus-end tracking

Quantitative MT plus-end tracking ratio analyses reveal severe defects in the INT-inactivated mutants. We measured the average and variance in the tracking ratios for the INT1, INT2, and INT1+2 using the approach described in Figure 4, A and B (details described in Supplemental Figure S13A). Tracking intensities, tracking durations, and MT growth durations for the INT mutants showed that each parameter fitted a mono-modal Gaussian distribution similar to wild-type and TOG-inactivated mutants (Supplemental Figure S14). Kymographs show the plus-end tracking signal intensity for these mutants regularly dropping below background levels during MT polymerization phases as shown in Figure 7A (additional example kymographs are shown in Supplemental Figure S13, B–D). The average tracking times for these mutants were roughly 30% decreased compared with wt-Alp14 (Supplemental Figure S14D). Figure 6B shows average tracking ratios and their variance (analysis described in Supplemental Figure S14), revealing that INT1 exhibited a low tracking

FIGURE 5: Interfaces stabilizing the TOG square assembly are critical for MT polymerase and plus-end tracking activities in vivo. (A) Model of structural defects in organization of TOG square assembly in the INT-inactivated mutants as described in (Nithianantham *et al.*, 2018). Left, wt-Alp14 forms a square assembly with TOG1 binding tightly to tubulin and TOG2 exchanging tubulin rapidly. The INT1 mutant destabilizes interface 1 leading to isolated TOG1-TOG2 subunits. INT2 mutant inactivates interface 2 leading defect within each TOG1-TOG2 organization in each subunit. INT1+2 has defects in both interfaces 1 and 2. (B) Images of *S. pombe* cells expressing INT1, INT2, or INT1+2 Alp14 mutants. Top, raw cell images with MTs marked with mCherry-Atb2 tubulin (red) and Alp14-GFP (green). Bottom, kymographs of dynamic MTs and Alp14-GFP. White arrows, beginnings of abnormal MT tracking events; blue arrows, ends of such events. Additional examples are shown in Supplemental Figure S10A. (C) MT polymerization rate spreads in wt cells (3.2 μm/min), INT1 (2.6 μm/min), INT2 (2.4 μm/min), and INT1+2 (2.3 μm/min) (Supplemental Table S3). *t* Tests were performed to compare the control to each condition and the *p* value is reported for each comparison marked. Error bars represent SD of the condition. (D) Proportion of dynamic MTs with abnormal tracking behavior in each strain. INT1, INT2, and INT1+2M have higher ratios of these events compared with cells harboring wt-Alp14. (E) Distribution and average of Alp14-GFP intensities at growing MT plus ends in each strain. INT1, INT2, INT1+2 strains all show lower intensities than wt cells at MT plus ends. *t* Tests were performed to compare the control to each condition, and the *p* value is reported for each comparison marked. Error bars represent SD of the condition. (F) MT plus-end tracking ratios for Alp14 signal revealing defects in the persistence of mutants at polymerizing MT plus ends. Analysis is a result of data shown in Supplemental Figure S11. Values are reported in Supplemental Table S3. *t* Tests were performed to compare the control to each condition. The *p* value is reported for each comparison marked. Error bars represent SD of the condition. Data on wt-Alp14 in C–F are the same as for wt-Alp14 in Figure 2, C–F.

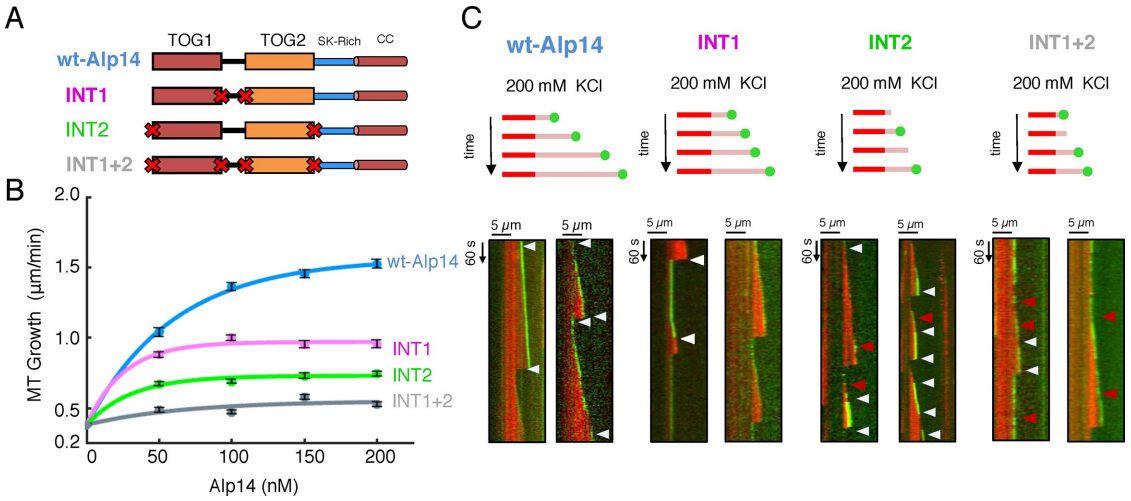

FIGURE 6: Inactivation of TOG square assembly interfaces proportionally inactivates both MT polymerase and MT plus-end tracking in vitro. (A) Alp14 linear domain Alp14 constructs showing the domain organization. The red X indicates the location of inactivating interfaces through point mutations as described previously (Nithianantham *et al.*, 2018). (B) MT polymerase activities of wt, INT1, INT2, and INT1+2 constructs at 200 mM KCl. INT1 shows a 50% decrease in MT polymerase compared with wt-Alp14, whereas INT2 and INT1+2 show a 75% decrease in MT polymerase activity (90%) compared with wt-Alp14. MT polymerization rates are reported in Supplemental Table S1. The curves were fitted using the exponential function a-b*e(-c*x). Error bars represent the SEM of each point. (C) Top, model for the observed Alp14 localization and MT polymerization activity; bottom, kymographs of individual dynamic MTs with wt-Alp14 or mutants at 200 mM KCl. White arrowheads denote beginning and end of tracking events, and red arrowheads denote rapid binding and dissociation events.

ratio with high variance (average 76.4; range 84.3%). INT2 exhibited a further decrease in tracking ratio and very high variance (average 66.4%; range 97.5%). INT1+2 also exhibited a similarly low tracking ratio with high variance (average 78.3%; range 86.1; Figure 7B). The low tracking ratios and extensive variance in the plus-end tracks indicate that these INT mutants have poor persistence in tracking polymerizing MT plus ends and dissociate randomly from MT plus ends.

Single molecule tracking measurements revealed cumulative defects in the INT-inactivated mutants, increasing in severity from INT1 to INT1+2 correlating with number of mutated interfaces. Using the approach described in Figure 4C, single molecule tracking events were identified in kymographs (Figure 7C; Supplemental Figure S15; Supplemental Movie S4). The INT1 and INT2 dwell times were measured at 79.8 s ($n = 112$) and 77.3 s ($n = 112$), respectively. These dwell times were 40% lower than wt-Alp14 (Figure 7C). The INT1+2 showed a cumulative defect with a further decrease in dwell time to 55.2 s ($n = 77$), which was roughly 67% lower than wt-Alp14 and ~27% lower than either INT1 or INT2. On average, a single wt-Alp14 dimer molecule promoted the polymerization of ~422 αβ-tubulin subunits per event, INT1 promoted ~178 αβ-tubulin subunits, INT2 promoted ~128 αβ-tubulin subunits, and INT1+2 promoted ~93 αβ-tubulin subunits (Supplemental Table S2). Thus, our analyses suggest that each type of interface plays a role in processive MT plus-end tracking, and that these tracking defects correlated directly with the severity observed for the decrease in Alp14 MT polymerase activity in these mutants.

DISCUSSION

Origin of MT polymerase and plus-end tracking within TOG array features

Our in vitro and in vivo studies of the two Alp14 mutant classes reveal a distinct relationship between the Alp14 MT polymerase and processive MT plus-end tracking activities and suggest how these functions arise from specific features conserved of TOG arrays. TOG1 and TOG2 represent two distinct classes of domains which differ in their affinities for αβ-tubulin and their positions within the arrays (Ayaz *et al.*, 2014; Nithianantham *et al.*, 2018). Our data support the idea that soluble αβ-tubulins recruited by TOG1 and TOG2 are essential for a concerted polymerization mechanism, consistent with other studies (Widlund *et al.*, 2011; Geyer *et al.*, 2018). However, we show using a variety of approaches that the contributions of TOG1 and TOG2 are not equivalent in MT polymerase and processive MT plus-end tracking activities. Compared with TOG2, TOG1 is more critical for processive MT plus-end tracking and makes a smaller contribution to MT polymerase activity, and its inactivation is functionally less severe in vivo. Whereas TOG2 is more critical for MT polymerase and plays a smaller role in MT plus-end tracking, its inactivation is functionally more severe in vivo.

TOG domains recruit and incorporate αβ-tubulins into MTs via a catch and release mechanism (Ayaz *et al.*, 2012, 2014). The conserved TOG1 and TOG2 domains differ in their affinities for αβ-tubulin by roughly twofold at low ionic strength (70 and 173 nM for TOG1 and TOG2, respectively, at 50–100 mM KCl). One caveat is that we utilized porcine αβ-tubulin instead of *S. pombe* αβ-tubulin for our in vitro MT dynamics reconstitution studies. However, the affinities of Alp14 TOG1 and TOG2 for porcine αβ-tubulin are nearly identical to those measured for *Saccharomyces cerevisiae* Stu2 TOG1 and TOG2 in binding to *S. cerevisiae* αβ-tubulin. These nearly identical affinities support the conservation and unique interfaces of TOG1 and TOG2 in binding αβ-tubulin (Ayaz *et al.*, 2014; Nithianantham *et al.*, 2018). Furthermore, *S. pombe* αβ-tubulin was demonstrated to exhibit a similar critical concentration for polymerization as porcine αβ-tubulin, unlike *S. cerevisiae* αβ-tubulin, which exhibits a fivefold lower polymerization critical concentration (Podolski *et al.*, 2014; Hussmann *et al.*, 2016). Thus, despite the use of porcine αβ-tubulin in our in vitro MT dynamics reconstitution studies, porcine αβ-tubulin is not likely to influence the patterns of

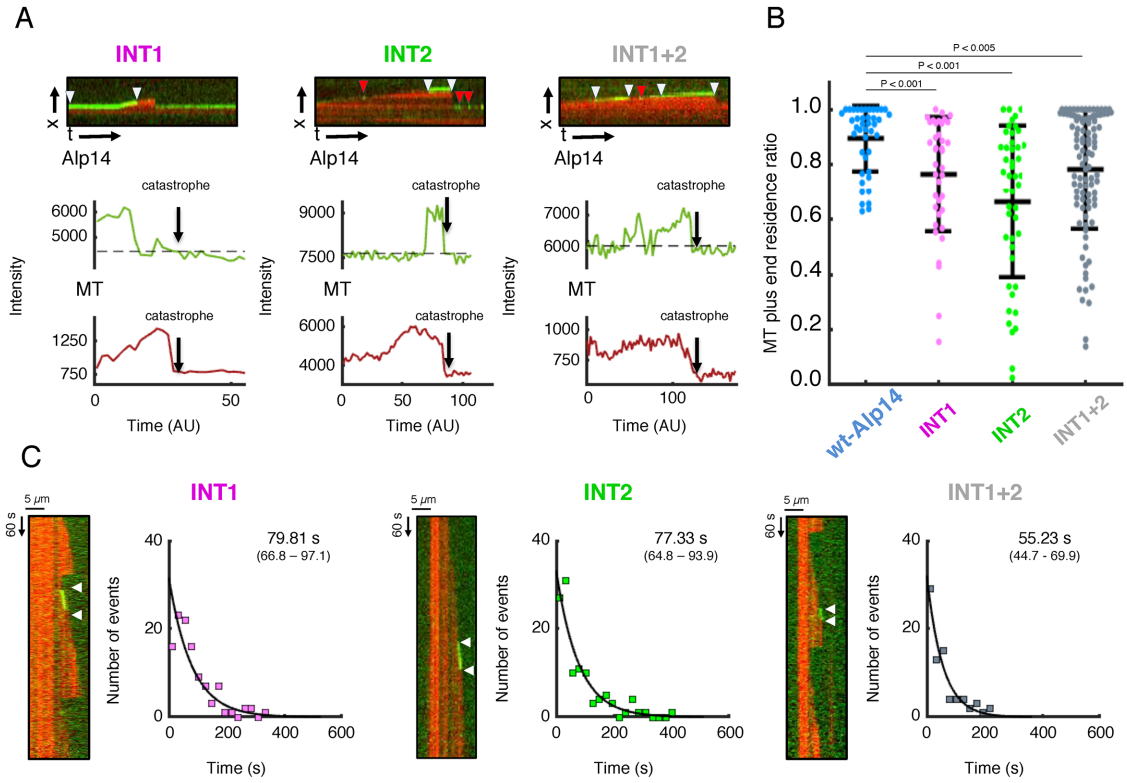

FIGURE 7: TOG Square assembly interfaces are collectively critical for processive MT plus-end tracking. (A) Example tracking ratio measurements for INT1, INT2, and INT1+2 at MT plus ends. Top, horizontal kymograph; middle, Alp14 bulk signal intensity that is above background (broken line); bottom, MT plus-end intensity throughout the polymerization phase up to catastrophe (arrow) above background (broken line). Note that unlike wt-Alp14, INT1, INT2, and INT1+2 signal reveal progressively decreased MT plus-end tracking through rapid dissociations. Additional examples are shown in Supplemental Figure S13. (B) Tracking ratios at MT plus-end INT1, INT2, and INT1+2 compared with wt-Alp14. This is a result of analysis described in Supplemental Figure S14. *t* Tests were performed to compare the control to each condition. The *p* value is reported for each comparison marked. Error bars represent SD of the condition. (C) Single-molecule dynamic MT polymerization studies reveal the average dwell time for INT1, INT2, and INT1+2 mutants. Left, example kymographs; right, binned dwell-time frequencies fitted to an exponential decay. Additional examples are shown in Supplemental Figure S15.

MT polymerase and plus-end tracking defects seen in the Alp14 mutants. This is further supported by the similarity of the in vitro results with the in vivo results observed in *S. pombe* (Figures 2–4).

Our findings clarify the role of TOG domains in the catch and release of tubulin by TOG domains for MT polymerization. We measured the TOG1 and TOG2 affinities for αβ-tubulin decrease 20-fold when the solution's ionic strength is increased from 50 to 200 mM KCl. We show that enhancing the αβ-tubulin affinity for TOG1 and TOG2 at 50 mM KCl directly slows Alp14 MT polymerase rates. At 50 mM KCl, the wt-Alp14 MT polymerase is 40% lower than its activity at 200 mM KCl. The TOG1M and TOG2M defects observed at 200 mM KCl further diverge at 50 mM KCl, where the TOG2M shows a far more severe phenotype than TOG1M (Figure 3). These data directly support the catch and release mechanism for TOG domains, since MT polymerase rates directly correlate with αβ-tubulin release rates (Ayaz *et al.*, 2012, 2014). Our data reveal the rapid release of αβ-tubulin from TOG domains directly enhances MT polymerase activity. Although enhancing TOG affinities at 50 mM KCl leads to longer tracks for TOG1M, its MT polymerase decreases by only 30%, whereas TOG2M at 50 mM KCl conditions retains efficient and long MT plus-end tracks with an 83% decrease in MT polymerase. Therefore, the αβ-tubulins recruited and incorporated by TOG1 and TOG2 contribute very differently to MT plus-end tracking and MT polymerase functions.

Through the INT-inactivated mutants, we show that assembly of TOG arrays into the TOG square assembly is essential for both MT polymerase and plus-end tracking functions (Nithianantham *et al.*, 2018). Inactivating the TOG square interfaces in the INT1, INT2, and INT1+2 mutants lead either to premature αβ-tubulin polymerization or to disorganized arrays with unpolymerized αβ-tubulins (Figure 5A) (Nithianantham *et al.*, 2018). Our studies reveal a direct relationship between the severity of defects in MT polymerase and the defects observed in plus-end tracking in these INT-inactivated mutants. These mutants exhibit unique tracking defects characterized by rapid association and dissociation with MT plus ends. Despite their normal abilities to bind αβ-tubulin in vitro, the INT-inactivated mutants show defects in processive MT plus-end tracking with cumulative severity, which correlated with the severity levels in their MT polymerase defects (Nithianantham *et al.*, 2018).

Comparing MT polymerase and plus-end tracking features to the in vivo setting

Our in vivo studies suggest that the TOG array features are important for MT polymerase and plus-end tracking functions within living cells. The unique contributions of TOG1 and TOG2 αβ-tubulin recruiting activities to the MT polymerase and plus-end tracking functions in the in vitro studies become even more pronounced in the in vivo setting (Figure 2). TOG2 is functionally essential for MT

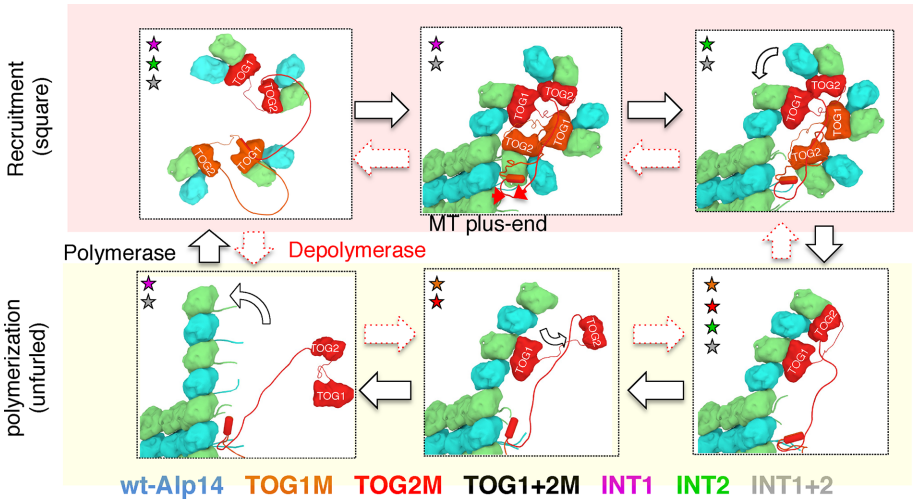

FIGURE 8: A processive cycle describes the relation of plus-end tracking to MT polymerase, and their origin from features of TOG arrays. Two states of the dynamic MT polymerase dynamic cycle: recruitment mediated by TOG square state (red boundary) and polymerization mediated by the unfurled state (yellow boundary). The transition from each state to the next is being disrupted by different Alp14 mutants (denoted by stars).

polymerase activity and its inactivation is nearly equivalent to inactivating both TOG1 and TOG2, as revealed by both survival assays and MT polymerization rates. In contrast, the MT plus-end tracking function of Alp14 in vivo more critically depends on TOG1 than on TOG2. TOG2M has similar MT plus-end tracking activity to wt-Alp14, whereas TOG1M tracks MT plus ends with poor persistence. Surprisingly, TOG1+2M retains MT plus-end tracking despite its severely asynchronous defect in vivo and is contrary to the lack of any tracking for this mutant in vitro (Figure 2).

Inactivating TOG square interfaces leads to defects in Alp14 MT polymerase and plus-end tracking in vivo. However, in vivo, the MT polymerase defects in the INT1, INT2 and INT1+2 mutants (Figure 5) are less severe than those observed in the in vitro setting (Figure 6). An important question arises from these comparisons: What are the reasons for the differences in severity of INT-inactivated and TOG1+2M defects observed in vitro compared with the in vivo studies? In living cells, a secondary MT plus-end localization pathway may compensate for these defects in the mutant Alp14 proteins. Alp14 exists in complex with Alp7, an orthologue of the transforming acidic coiled-coil protein class, which may enhance Alp14 MT plus-end tracking efficiency (Flor-Parra *et al.*, 2018). Future studies with Alp14-Alp7 may revolve on solving these questions directly. It also remains unknown whether there are cellular factor(s) that may stabilize the TOG square assembly in vivo, which may mitigate the INT-inactivated defects.

A MT polymerase polarized unfurling catalytic cycle

The functional and reconstitution data presented here validate all aspects of the polarized unfurling model and are fully consistent with all its facets (Nithianantham *et al.*, 2018) (Figure 1B). Our studies show that TOG1 and TOG2 domains function cooperatively yet serve distinct roles in MT plus-end tracking and MT polymerase, respectively. The asymmetric organization of the TOG square produces steric hindrance when a TOG1-αβ-tubulin docks onto MT plus ends. This unfurling of TOG arrays into the polymerization state leads TOG1-αβ-tubulin to occupy the position closer to the MT plus end, while TOG2-αβ-tubulin occupies a position at the end of the newly formed protofilament which lies above TOG1-αβ-tubulin (Figure 8) (Nithianantham *et al.*, 2018). The sequential nature of unfurling and polymerization of TOG2-αβ-tubulin, following the docking of TOG1-αβ-tubulin, leads to these distinct positions (Figure 8B). Our data directly support that processive MT plus-end tracking critically depends on TOG1-αβ-tubulin docking and requires interfaces 1 and 2 to stabilize the TOG square (described in Figure 8). This is also consistent with the idea that reformation of the TOG square assembly is critical for processive MT plus-end tracking (Figure 8). The MT polymerase function critically requires TOG2-αβ-tubulin rotating around interface 2 following the docking TOG1-αβ-tubulin; it also requires the TOG square assembly interface 1 for full polymerase function (Figure 7B). These data and the polarized unfurling model explain the specific relationship between the MT polymerase and plus-end tracking functions within the features of the TOG arrays. (Nithianantham *et al.*, 2018).

How the mutant defects fit within the polarized unfurling model

A synthesis of the defects observed in both TOG- and INT-inactivated mutants suggests that both the TOG square and the polymerized states are critical for MT polymerase and processive MT plus-end tracking (Figure 8). Data from single molecule studies support the idea that processive activity is likely due to cycling between these two states: the TOG square mediates αβ-tubulin recruitment in solution and then unfurls to the extended state, which promotes αβ-tubulin polymerization (Figure 8). This cycle involves forming the square assemblies to reload with soluble αβ-tubulins from the cytoplasm after each round of polymerization at MT plus ends. During reloading, the SK-rich region maintains association with the MT lattice, while the TOG domains are free to bind αβ-tubulins. The proximity of the SK rich-region to TOG square-αβ-tubulin docking at MT plus-end is critical during MT polymerase cycle as shown by a recent study using Stu2 chimeras (Geyer *et al.*, 2018). The distinct contributions of αβ-tubulin recruited by TOG1 and TOG2 to the MT plus-end tracking and MT polymerase function stem from their sequential polymerization following docking. Different steps in this catalytic cycle may be affected by the different types of mutants studied here (Figure 8). INT1, INT2, and INT1+2 mutants cripple TOG square assembly, and TOG1M disrupts its docking at MT plus ends. On the other hand, INT2, TOG1M, TOG2M, and TOG1+2M disable formation of the polymerization state (Figure 8). It is notable that INT2 and TOG1M share defects in both states due to influencing MT plus-end docking or the unfurling following docking, respectively (Figure 8) (Nithianantham *et al.*, 2018).

Our studies also show that all the features of TOG array that make up the MT polymerase are also essential for accelerating MT depolymerization in vivo. In MT depolymerase activity, the catalytic cycle operates in reverse at the depolymerizing MT plus ends. The extend state forms at curved protofilaments, then furls to dissociate individual αβ-tubulins by forming the TOG square state (Figure 8). The MT depolymerase and polymerase activities of TOG arrays likely increase the dynamic cycling necessary for reorganization of the MT network during mitosis (Shirasu-Hiza *et al.*, 2003; van Breugel *et al.*, 2003).

Comparison to other MT polymerase models

Two alternate models for TOG arrays as MT polymerases have been presented by other groups. In one model, TOG arrays recruit αβ-tubulins and release them on polymerization without forming assemblies. In this model, TOG arrays stimulate polymerization by increasing local concentration of αβ-tubulin at MT plus ends, potentially promoting lateral αβ-tubulin interactions (Ayaz *et al.*, 2014). In a second model, TOG arrays promote formation of protofilament-like tubulin polymers in solution and then dock these polymerized tubulins onto MT plus ends, where TOG1 resides at the outermost αβ-tubulin in the new protofilament, whereas TOG2 and other domains bind to αβ-tubulins polymerized within the MT lattice (Byrnes and Slep, 2017).

The first model was recently tested by studying TOG-inactivated mutants and chimeras that include all-TOG1 or all-TOG2 Stu2 constructs (Geyer *et al.*, 2018). This work suggests that TOG domain identities are not critical for MT polymerase activity as long as two TOG domains are linked within a single subunit array and bind the MT lattice via the SK-rich region. Specifically, the conclusions rest on the assumption that the engineered Stu2 constructs fully disrupt any higher-order assembly capacity within the TOG arrays, and that those are only mediated by the unique interactions of TOG1 and TOG2 domains. Although αβ-tubulin binding and organization of these engineered TOG arrays were not measured, based on our square assembly x-ray structure and the regions swapped to form these Stu2 chimera constructs, it is likely that a linker element N-terminal to TOG2, which is critical for forming the square assembly state with TOG1, remains and may be sufficient for TOG square assembly in these mutants (Geyer *et al.*, 2018; Nithianantham *et al.*, 2018). Thus, despite TOG domain swaps in these chimera constructs, the constructs may therefore still retain some capacity for forming TOG square assemblies.

Although the two other models support the cooperative roles for TOG1 and TOG2 in the polymerase activity (Byrnes and Slep, 2017; Geyer *et al.*, 2018), they cannot explain the unique contributions of TOG1 and TOG2 domains to MT polymerase and processive MT plus-end tracking functions that are revealed in this study. The other models suggest that only αβ-tubulin recruiting activities by TOG1 and TOG2 are necessary and sufficient for MT polymerase, and that this recruiting activity is directly proportional to MT plus-end tracking activity (Brouhard and Rice, 2018). These models suggest that mutations that do not affect αβ-tubulin binding would not influence MT polymerase or plus-end tracking. In contrast, our studies of the INT-inactivated mutants show that interfaces that stabilize TOG square assemblies, without influencing αβ-tubulin binding, are critical for processive MT plus-end tracking and MT polymerase activity (Figure 8) (Nithianantham *et al.*, 2018).

Conclusion

Our combined in vivo and in vitro studies assign the origins of the MT polymerase and MT plus-end tracking functions to the affinity of the TOG1 and TOG2 domains for αβ-tubulins and square assembly features of TOG arrays. Combined with the polarized unfurling model, our data suggest that a dynamic cycle between the TOG square recruitment and the unfurled polymerization states of XMAP215/Stu2/Alp14 proteins likely drives processive activity at MT plus ends.

MATERIALS AND METHODS

Cloning of Alp14 mutants

The cDNA regions encoding *S. pombe* Alp14 or each of its six mutants were generated as shown schematically in Supplemental Figures S1A and S8A. Full-length Alp14 genes were used for the in vivo studies, whereas Alp14 constructs including residues 1–690 were used for in vitro studies. Details for how Alp14 and its point mutants were generated are given in the Supplemental Materials and Methods.

Generation of *S. pombe* Alp14 mutant strains

S. pombe strains are described in Supplemental Table S4 and were generated by replacing the endogenous Alp14 locus with mutant *alp14* genes, as described in the Supplemental Materials and Methods. Survival and drop assays for these mutants are also described in the Supplemental Materials and Methods.

Imaging and analysis of Alp14 and MTs in *S. pombe* cells

Live-cell imaging on *S. pombe* mutant strains was performed at 25°C as described in the Supplemental Materials and Methods using a spinning-disk confocal microscope and Metamorph software. Image stacks were analyzed using ImageJ version 1.74q as detailed in the Supplemental Materials and Methods. Tracking ratios were determined as shown (Supplemental Figures S2–S4, A and C, and S11, A and C). Details of the tracking measurement calculations are given in the Supplemental Materials and Methods. Graphs and statistical analyses were performed using GraphPad Prism version 5.0 (GraphPad Software). Live Imaging for wt and all mutant cell strains was carried out in parallel using the same imaging conditions. For the wt or mutant cell strain, multiple imaging data sets were collected using the same imaging conditions.

Purification of Alp14 and mutants

Expression and purification of Alp14 for in vitro studies were performed using the approach described previously (Nithianantham *et al.*, 2018) with modifications described in detail in the Supplemental Materials and Methods.

In vitro dynamic MT polymerization assays

MT polymerase activity with dynamic MTs was reconstituted and carried out as described previously (Al-Bassam *et al.*, 2012) with the modifications described in the Supplemental Materials and Methods.

Analysis of MT dynamic polymerization parameters and tracking ratios

Movies for dynamic MTs using the program FIJI (Schindelin *et al.*, 2012) used the approach detailed in the Supplemental Materials and Methods. Tracking ratios were calculated from kymographs of dynamic MT plus ends with 200 nM Alp14-mNG or its mutants by measuring line scans of the MT plus ends in the 633 and 488 nm emission channels and performing an automated analysis, as described in the Supplemental Materials and Methods.

Single-molecule TIRF assays to measure MT plus-end binding dynamics

Single-molecule TIRF assays were performed by a modified approach to the bulk TIRF assays using the SNAPf-tagged Alp14 constructs (Alp14-SNAP). Protein labeling with dyes, reconstitution, and imaging approaches and analyses are all detailed in the Supplemental Materials and Methods.

Statistical analysis

Statistical analyses were performed in MATLAB. The Student's *t* test was used to compare each condition to the wild-type conditions. MT growth measurements were fitted using an exponential function

a-b*e(-c*x). Single molecule dwell time measurements were fitted to a first-order exponential decay function.

ACKNOWLEDGMENTS

We thank Stanley Nithianantham for suggestions, Qianyan Li and In Young Choi for project support, Richard J. Mckenney, Kassandra Ori-McKenney, Frank J. McNally, and Jodi Nunnari (Molecular Cellular Biology) for suggestions and support, Bruce Goode and Jessica Henty-Ridilla (Brandeis University) for suggestions on surface treatment protocols, Refael Daga (Universidad Pablo De Olavide) laboratory for suggestions and support. B.D.C. was supported by the UC Davis Training Program in Molecular and Cellular Biology (funded in part by NIH-T32-GM007377). J.A.-B. is supported by NIH-GM110283 and NSF-1615991. I.F.-P. is supported by the research program funds from the Universidad Pablo De Olavide. F.C. is supported by NIH-GM115185.

REFERENCES

Akhmanova A, Steinmetz MO (2011). Microtubule end binding: EBs sense the guanine nucleotide state. Curr Biol 21, R283–R285.

Akhmanova A, Steinmetz MO (2015). Control of microtubule organization and dynamics: two ends in the limelight. Nat Rev Mol Cell Biol 16, 711–726.

Al-Bassam J, Chang F (2011). Regulation of microtubule dynamics by TOG-domain proteins XMAP215/Dis1 and CLASP. Trends Cell Biol 21, 604–614.

Al-Bassam J, Kim H, Flor-Parra I, Lal N, Velji H, Chang F (2012). Fission yeast Alp14 is a dose-dependent plus end-tracking microtubule polymerase. Mol Biol Cell 23, 2878–2890.

Al-Bassam J, van Breugel M, Harrison SC, Hyman A (2006). Stu2p binds tubulin and undergoes an open-to-closed conformational change. J Cell Biol 172, 1009–1022.

Asbury CL (2008). XMAP215: a tip tracker that really moves. Cell 132, 19–20.

Ayaz P, Munyoki S, Geyer EA, Piedra FA, Vu ES, Bromberg R, Otwinowski Z, Grishin NV, Brautigam CA, Rice LM (2014). A tethered delivery mechanism explains the catalytic action of a microtubule polymerase. Elife 3, e03069.

Ayaz P, Ye X, Huddleston P, Brautigam CA, Rice LM (2012). A TOG:alphabeta-tubulin complex structure reveals conformation-based mechanisms for a microtubule polymerase. Science 337, 857–860.

Brouhard GJ, Rice LM (2014). The contribution of alphabeta-tubulin curvature to microtubule dynamics. J Cell Biol 207, 323–334.

Brouhard GJ, Rice LM (2018). Microtubule dynamics: an interplay of biochemistry and mechanics. Nat Rev Mol Cell Biol 19, 451–463.

Brouhard GJ, Stear JH, Noetzel TL, Al-Bassam J, Kinoshita K, Harrison SC, Howard J, Hyman AA (2008). XMAP215 is a processive microtubule polymerase. Cell 132, 79–88.

Byrnes AE, Slep KC (2017). TOG-tubulin binding specificity promotes microtubule dynamics and mitotic spindle formation. J Cell Biol 216, 1641–1657.

Flor-Parra I, Iglesias-Romero AB, Chang F (2018). The XMAP215 ortholog Alp14 promotes microtubule nucleation in fission yeast. Curr Biol 11, 1681–1691.

Garcia MA, Vardy L, Koonrugsa N, Toda T (2001). Fission yeast ch-TOG/XMAP215 homologue Alp14 connects mitotic spindles with the kinetochore and is a component of the Mad2-dependent spindle checkpoint. EMBO J 20, 3389–3401.

Geyer EA, Miller MP, Brautigam CA, Biggins S, Rice LM (2018). Design principles of a microtubule polymerase. Elife 7, e34574.

Haase KP, Fox JC, Byrnes AE, Adikes RC, Speed SK, Haase J, Friedman B, Cook DM, Bloom K, Rusan NM, Slep KC (2018). Stu2 uses a 15-nm parallel coiled coil for kinetochore localization and concomitant regulation of the mitotic spindle. Mol Biol Cell 29, 285–294.

Hussmann F, Drummond DR, Peet DR, Martin DS, Cross RA (2016). Alp7/TACC-Alp14/TOG generates long-lived, fast-growing MTs by an unconventional mechanism. Sci Rep 6, 20653.

Kakui Y, Sato M, Okada N, Toda T, Yamamoto M (2013). Microtubules and Alp7-Alp14 (TACC-TOG) reposition chromosomes before meiotic segregation. Nat Cell Biol 15, 786–796.

Maurer SP, Bieling P, Cope J, Hoenger A, Surrey T (2011). GTPgammaS microtubules mimic the growing microtubule end structure recognized by end-binding proteins (EBs). Proc Natl Acad Sci USA 108, 3988–3993.

Maurer SP, Cade NI, Bohner G, Gustafsson N, Boutant E, Surrey T (2014). EB1 accelerates two conformational transitions important for microtubule maturation and dynamics. Curr Biol 24, 372–384.

Nithianantham S, Cook BD, Beans M, Guo F, Chang F, Al-Bassam J (2018). Structural basis of tubulin recruitment and assembly by microtubule polymerases with tumor overexpressed gene (TOG) domain arrays. Elife 7, e38922.

Okada N, Toda T, Yamamoto M, Sato M (2014). CDK-dependent phosphorylation of Alp7-Alp14 (TACC-TOG) promotes its nuclear accumulation and spindle microtubule assembly. Mol Biol Cell 25, 1969–1982.

Podolski M, Mahamdeh M, Howard J (2014). Stu2, the budding yeast XMAP215/Dis1 homolog, promotes assembly of yeast microtubules by increasing growth rate and decreasing catastrophe frequency. J Biol Chem 289, 28087–28093.

Sato M, Toda T (2007). Alp7/TACC is a crucial target in Ran-GTPase-dependent spindle formation in fission yeast. Nature 447, 334–337.

Sato M, Vardy L, Angel Garcia M, Koonrugsa N, Toda T (2004). Interdependency of fission yeast Alp14/TOG and coiled coil protein Alp7 in microtubule localization and bipolar spindle formation. Mol Biol Cell 15, 1609–1622.

Schindelin J, Arganda-Carreras I, Frise E, Kaynig V, Longair M, Pietzsch T, Preibisch S, Rueden C, Saalfeld S, Schmid B, *et al.* (2012). Fiji: an open-source platform for biological-image analysis. Nat Methods 9, 676–682.

Shirasu-Hiza M, Coughlin P, Mitchison T (2003). Identification of XMAP215 as a microtubule-destabilizing factor in Xenopus egg extract by biochemical purification. J Cell Biol 161, 349–358.

van Breugel M, Drechsel D, Hyman A (2003). Stu2p, the budding yeast member of the conserved Dis1/XMAP215 family of microtubule-associated proteins is a plus end-binding microtubule destabilizer. J Cell Biol 161, 359–369.

Widlund PO, Stear JH, Pozniakovsky A, Zanic M, Reber S, Brouhard GJ, Hyman AA, Howard J (2011). XMAP215 polymerase activity is built by combining multiple tubulin-binding TOG domains and a basic lattice-binding region. Proc Natl Acad Sci USA 108, 2741–2746.